SUPPLEMENTARY MATERIALS: Bulk modulus of Fe-rich olivines corrected for non hydrostaticity

Frédéric Béjina[a], Misha Bystricky[a], Nicolas Tercé[a], Matthew L. Whitaker[b,c,d], Haiyan Chen[b]

[a] *IRAP, Université de Toulouse, CNRS, CNES, UPS, 14 avenue Édouard Belin, 31400 Toulouse, France*
[b] *Mineral Physics Institute, Stony Brook University, Stony Brook, NY 11794-2100, USA*
[c] *Department of Geosciences, Stony Brook University, Stony Brook, NY 11794-2100 USA*
[d] *National Synchrotron Light Source II, Brookhaven National Laboratory, Upton, NY 11973 USA*

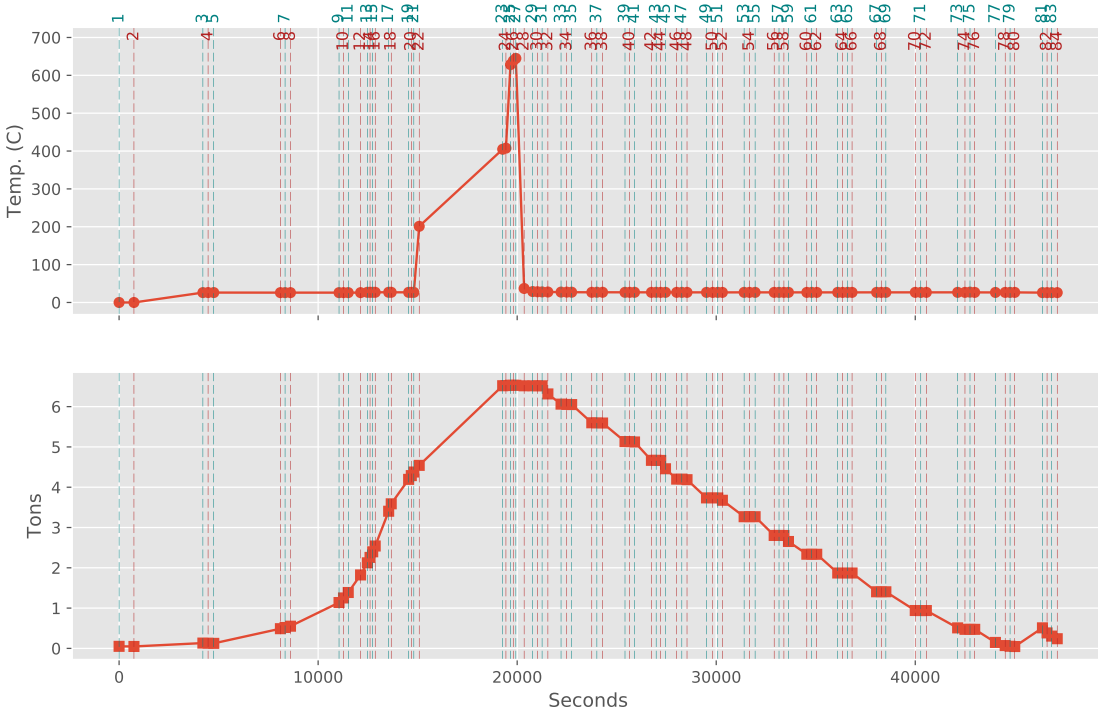

(a) Fa64

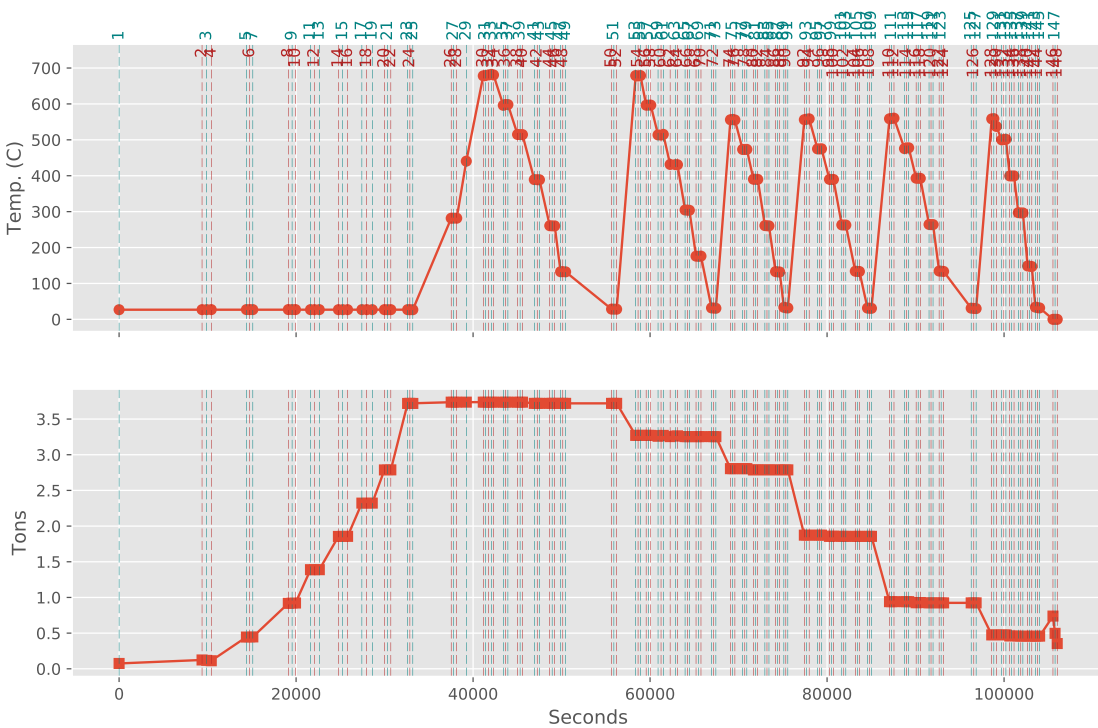

(b) Fa45

Figure S1: Tonnage and temperature paths followed during each experiment. Only results obtained at room T are presented in this paper. Numbers at the top of each graph are XRD pattern identification numbers (both NaCl and sample).

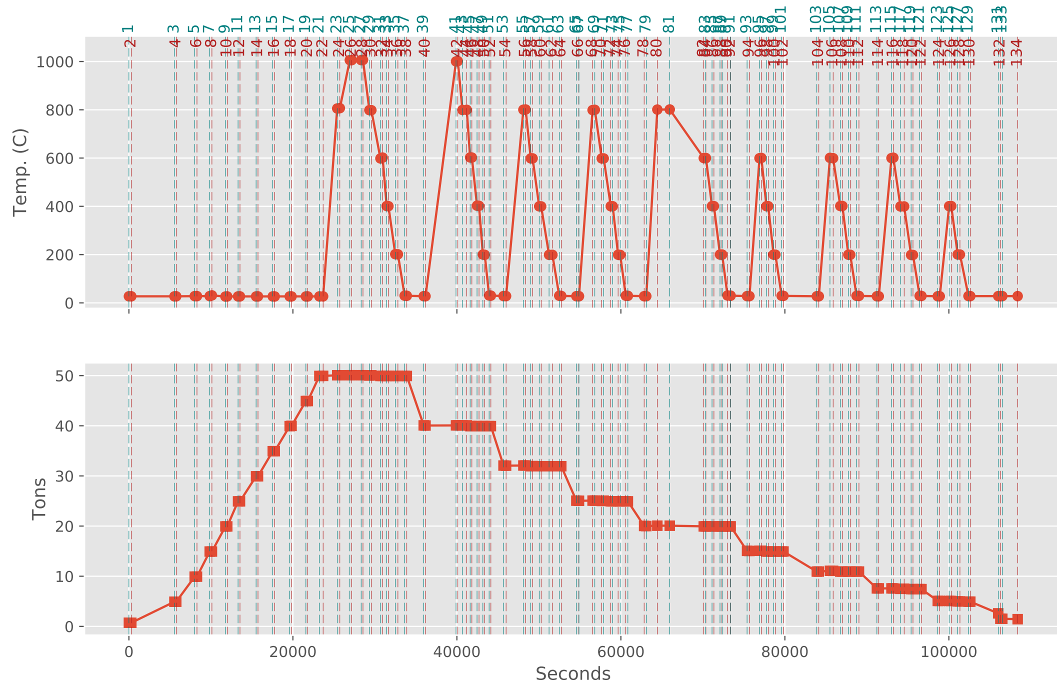

(c) Fa82

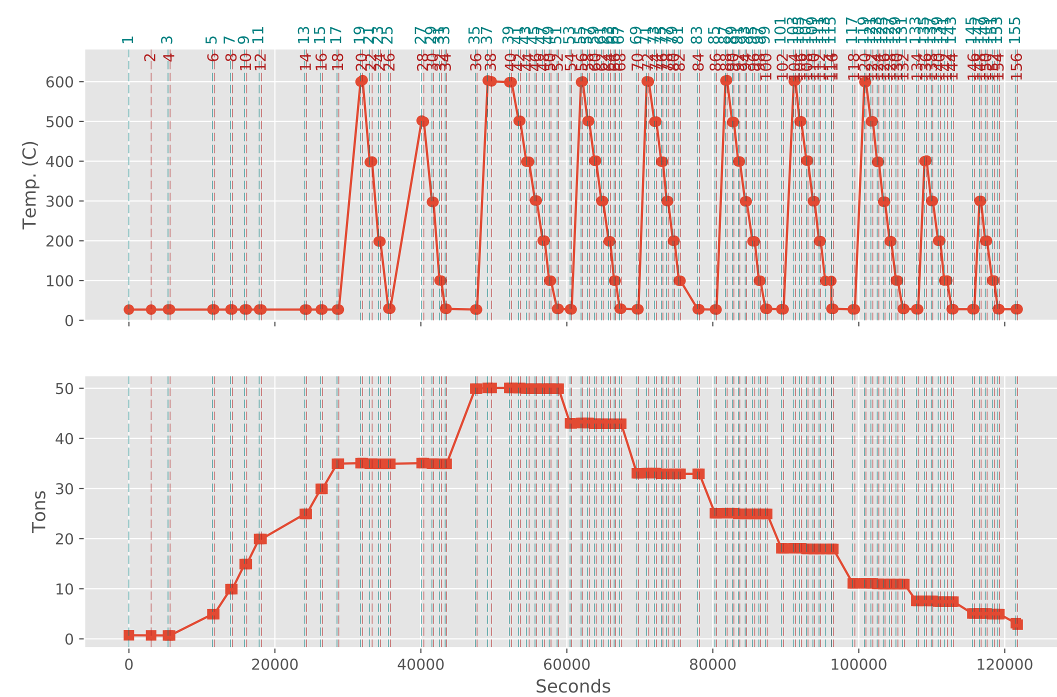

(d) Fa100

Figure S1: Tonnage and temperature paths followed during each experiment. Only results obtained at room T are presented in this paper. Numbers at the top of each graph are XRD pattern identification numbers (both NaCl and sample).

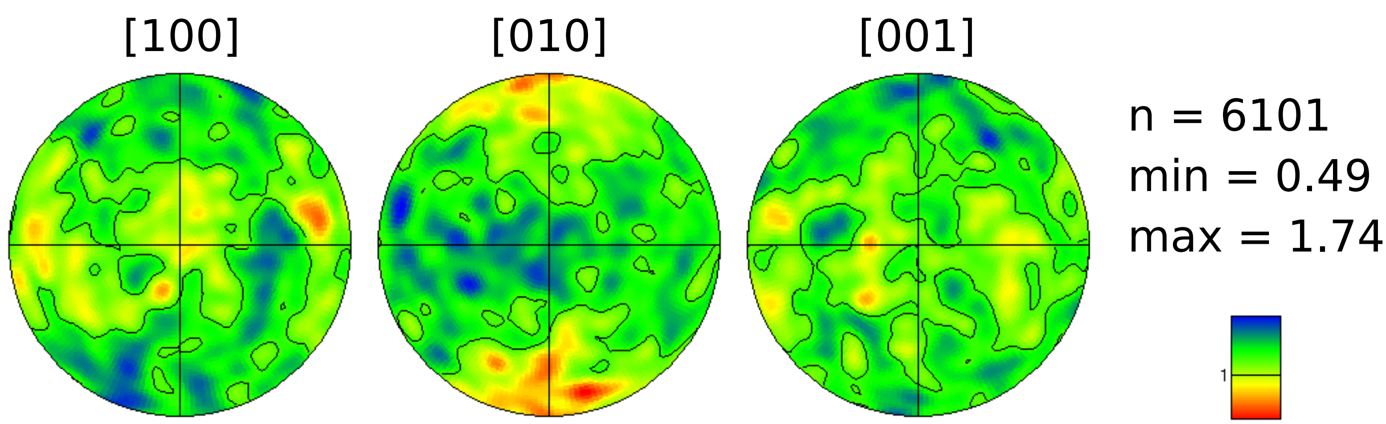

Figure S2: Pole figures for Fa82, representative of pole figures determined in all samples; upper hemisphere equal area projections oriented with the sample cylinder axis vertical. Discrete point distributions were smoothed with a Gaussian of 10° in Full Width Half Maximum. Pole figures are scaled in multiples of random distribution. The linear color scale extends from low intensities in blue to high intensities in red. Minima (min), maxima (max) and number of measurements (n; one point per grain) are indicated on the right.

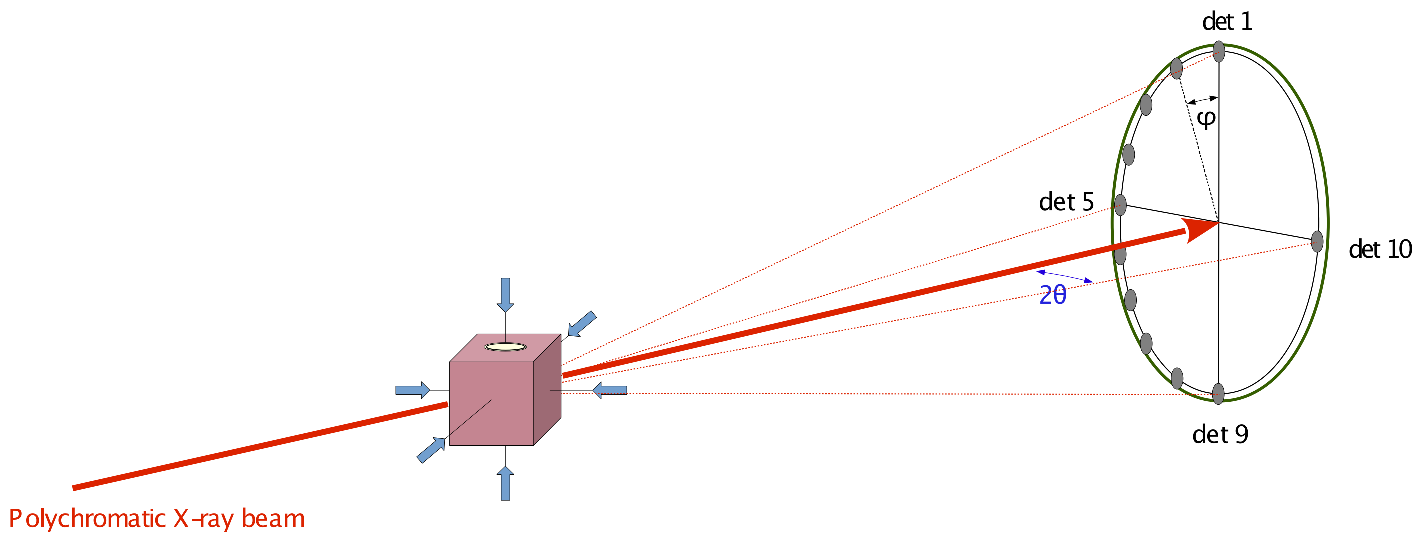

Figure S3: Schematic representation of the detection system used in our experiments. Detectors 1 to 9 are separated from one another by an azimuth angle, $\psi = 22.5°$. They recorded most of the XRD data. Detector 10 was usually only used for alignment of the system. Modified from Weidner et al. (2010, Fig. 3).

Table S1: Operational detectors.

Run#	Fa%	Detectors
AM309	45	1 to 9
AM215	64	1, 2, 6 to 10
AN400	82	3 to 9
AM313	100	1, 3 to 9

Table S2: P, V and t data for Fa45 and NaCl. d spacings are listed in file `fa45.csv`.

P (GPa)	V (Å^3)	t_{Fa45} (GPa)	P_{NaCl} (GPa)	V_{NaCl} (Å^3)	t_{NaCl} (GPa)
0.03 ± 0.02	297.488 ± 0.300	0.00 ± 0.01	0.03 ± 0.01	179.398 ± 0.023	0.00 ± 0.00
0.31 ± 0.06	296.922 ± 0.371	-0.28 ± 0.05	0.20 ± 0.01	178.217 ± 0.059	-0.12 ± 0.00
1.34 ± 0.08	294 ± 0.311	-0.47 ± 0.05	1.13 ± 0.00	172.327 ± 0.003	-0.15 ± 0.03
2.62 ± 0.07	291.109 ± 0.256	-0.46 ± 0.05	2.40 ± 0.01	165.805 ± 0.040	-0.12 ± 0.01
3.99 ± 0.21	288.258 ± 0.163	-0.10 ± 0.11	3.85 ± 0.05	159.839 ± 0.184	0.10 ± 0.05
4.97 ± 0.13	286.437 ± 0.253	-0.04 ± 0.02	4.84 ± 0.04	156.253 ± 0.144	0.17 ± 0.07
5.48 ± 0.04	286.3 ± 0.112	-0.88 ± 0.02	4.98 ± 0.01	155.693 ± 0.041	-0.14 ± 0.01
5.48 ± 0.06	286.402 ± 0.091	-1.02 ± 0.02	4.91 ± 0.03	155.923 ± 0.087	-0.17 ± 0.01
5.26 ± 0.06	286.934 ± 0.154	-0.94 ± 0.03	4.76 ± 0.02	156.469 ± 0.056	-0.19 ± 0.01
5.19 ± 0.09	287.18 ± 0.155	-1.14 ± 0.04	4.58 ± 0.02	157.055 ± 0.065	-0.22 ± 0.02
5.00 ± 0.08	287.696 ± 0.140	-1.15 ± 0.05	4.37 ± 0.02	157.813 ± 0.076	-0.20 ± 0.01
4.82 ± 0.06	288.183 ± 0.213	-1.21 ± 0.03	4.15 ± 0.01	158.639 ± 0.043	-0.21 ± 0.02
4.57 ± 0.08	288.827 ± 0.152	-1.23 ± 0.05	3.88 ± 0.01	159.623 ± 0.038	-0.19 ± 0.02
4.29 ± 0.06	289.338 ± 0.129	-1.30 ± 0.03	3.56 ± 0.01	160.873 ± 0.050	-0.21 ± 0.01
3.98 ± 0.11	289.943 ± 0.192	-1.36 ± 0.05	3.20 ± 0.01	162.316 ± 0.035	-0.18 ± 0.05
3.56 ± 0.12	290.705 ± 0.184	-1.30 ± 0.06	2.81 ± 0.01	163.972 ± 0.036	-0.17 ± 0.04
3.06 ± 0.04	291.597 ± 0.160	-1.20 ± 0.02	2.40 ± 0.01	165.825 ± 0.038	-0.21 ± 0.01
2.46 ± 0.10	292.554 ± 0.125	-1.02 ± 0.04	1.92 ± 0.01	168.164 ± 0.051	-0.20 ± 0.04
1.79 ± 0.07	293.911 ± 0.194	-0.81 ± 0.03	1.36 ± 0.02	171.029 ± 0.078	-0.17 ± 0.02
0.90 ± 0.08	295.774 ± 0.052	-0.58 ± 0.07	0.64 ± 0.01	175.331 ± 0.023	-0.19 ± 0.01
0.11 ± 0.08	297.58 ± 0.070	-0.05 ± 0.03	0.06 ± 0.01	179.242 ± 0.033	0.03 ± 0.04
0.01 ± 0.05	297.756 ± 0.219	0.02 ± 0.03	0.00 ± 0.01	179.629 ± 0.029	0.03 ± 0.02

Table S3: P, V and t data for Fa64 and NaCl. d spacings are listed in file `fa64.csv`.

P (GPa)	V (Å^3)	t_{Fa64} (GPa)	P_{NaCl} (GPa)	V_{NaCl} (Å^3)	t_{NaCl} (GPa)
0.03 ± 0.06	301.905 ± 0.261	0.03 ± 0.03	0.03 ± 0.02	179.824 ± 0.032	0.02 ± 0.02
0.03 ± 0.04	301.52 ± 0.232	0.07 ± 0.02	0.06 ± 0.02	179.663 ± 0.024	0.04 ± 0.01
1 ± 0.06	298.871 ± 0.191	-0.17 ± 0.02	0.88 ± 0.02	174.249 ± 0.022	0.02 ± 0.02
1.92 ± 0.08	296.944 ± 0.167	-0.2 ± 0.02	1.78 ± 0.04	169.186 ± 0.049	0.01 ± 0.03
2.78 ± 0.13	295.292 ± 0.2	-0.22 ± 0.03	2.63 ± 0.04	165.127 ± 0.042	0.01 ± 0.06
3.43 ± 0.18	294.281 ± 0.114	-0.16 ± 0.09	3.31 ± 0.05	162.209 ± 0.068	0.03 ± 0.03
4.09 ± 0.15	293.079 ± 0.191	-0.18 ± 0.05	3.92 ± 0.06	159.786 ± 0.079	0.07 ± 0.03
5.13 ± 0.13	291.105 ± 0.149	-0.1 ± 0.05	4.98 ± 0.05	156.036 ± 0.063	0.13 ± 0.02
3.37 ± 0.18	294.102 ± 0.128	-0.87 ± 0.06	2.83 ± 0.07	164.264 ± 0.069	-0.05 ± 0.05
2.99 ± 0.33	294.537 ± 0.171	-0.84 ± 0.06	2.59 ± 0.12	165.368 ± 0.104	-0.25 ± 0.16
2.91 ± 0.09	295.044 ± 0.127	-0.82 ± 0.05	2.44 ± 0.02	166.102 ± 0.014	-0.12 ± 0.01
0.49 ± 0.07	300.251 ± 0.15	-0.63 ± 0.05	0.1 ± 0.01	179.517 ± 0.075	-0.05 ± 0.02
0.03 ± 0.07	301.479 ± 0.147	-0.04 ± 0.03	0 ± 0.02	180.007 ± 0.026	0 ± 0.02

Table S4: P, V and t data for Fa82 and NaCl. d spacings are listed in file `fa82.csv`.

P (GPa)	V (Å^3)	t_{Fa82} (GPa)	P_{NaCl} (GPa)	V_{NaCl} (Å^3)	t_{NaCl} (GPa)
-0.02 ± 0.04	304.655 ± 0.035	-0.01 ± 0.01	-0.03 ± 0.01	179.611 ± 0.03	0 ± 0.01
0.49 ± 0.09	303.562 ± 0.033	-0.15 ± 0.03	0.37 ± 0.01	176.823 ± 0.025	0.03 ± 0.05
1.36 ± 0.04	301.8 ± 0.031	0.12 ± 0.01	1.35 ± 0.02	170.897 ± 0.041	0.13 ± 0.01
2.18 ± 0.08	300.196 ± 0.07	0.38 ± 0.05	2.33 ± 0.02	165.926 ± 0.036	0.16 ± 0.01
2.98 ± 0.08	298.482 ± 0.075	0.55 ± 0.05	3.21 ± 0.01	161.976 ± 0.015	0.19 ± 0.02
3.66 ± 0.11	297.036 ± 0.082	0.76 ± 0.08	4.04 ± 0.01	158.769 ± 0.006	0.2 ± 0.02
4.26 ± 0.13	295.657 ± 0.161	0.98 ± 0.09	4.76 ± 0.02	156.177 ± 0.019	0.23 ± 0.02
4.72 ± 0.15	294.798 ± 0.14	1.29 ± 0.1	5.44 ± 0.02	153.944 ± 0.025	0.2 ± 0.03
5.31 ± 0.17	293.6 ± 0.156	1.35 ± 0.14	6.08 ± 0.02	152.01 ± 0.015	0.2 ± 0.02
5.75 ± 0.2	292.573 ± 0.133	1.5 ± 0.15	6.63 ± 0.02	150.402 ± 0.01	0.18 ± 0.04
6.18 ± 0.28	291.517 ± 0.171	1.62 ± 0.21	7.14 ± 0.03	149.025 ± 0.019	0.19 ± 0.04
4.9 ± 0.19	294.202 ± 0.142	-0.38 ± 0.15	4.7 ± 0.02	156.442 ± 0.02	-0.09 ± 0.02
4.62 ± 0.08	294.814 ± 0.123	-0.55 ± 0.05	4.35 ± 0.01	157.638 ± 0.004	-0.14 ± 0.02
4.41 ± 0.16	295.527 ± 0.133	-0.55 ± 0.11	4.12 ± 0.02	158.536 ± 0.033	-0.11 ± 0.04
4.16 ± 0.14	296.18 ± 0.183	-0.64 ± 0.07	3.81 ± 0.02	159.652 ± 0.028	-0.12 ± 0.04
3.94 ± 0.14	296.538 ± 0.301	-0.62 ± 0.09	3.6 ± 0.02	160.463 ± 0.021	-0.12 ± 0.03
3.58 ± 0.2	297.065 ± 0.249	-0.68 ± 0.12	3.22 ± 0.03	161.977 ± 0.07	-0.13 ± 0.05
3.48 ± 0.2	297.47 ± 0.243	-0.74 ± 0.16	3.05 ± 0.02	162.73 ± 0.03	-0.09 ± 0.02
3.15 ± 0.12	297.988 ± 0.198	-0.76 ± 0.06	2.75 ± 0.02	164.006 ± 0.031	-0.15 ± 0.03
2.96 ± 0.17	298.604 ± 0.32	-0.72 ± 0.14	2.55 ± 0.01	164.925 ± 0.012	-0.11 ± 0.02
2.58 ± 0.13	299.113 ± 0.139	-0.76 ± 0.07	2.17 ± 0.03	166.683 ± 0.032	-0.14 ± 0.04
2.5 ± 0.09	299.464 ± 0.213	-0.8 ± 0.04	2.03 ± 0.01	167.366 ± 0.016	-0.1 ± 0.04
2.08 ± 0.13	300.507 ± 0.238	-0.8 ± 0.08	1.63 ± 0.01	169.367 ± 0.018	-0.12 ± 0.03
1.9 ± 0.09	300.988 ± 0.222	-0.79 ± 0.05	1.44 ± 0.02	170.401 ± 0.025	-0.1 ± 0.02
1.54 ± 0.13	301.457 ± 0.182	-0.81 ± 0.08	1.09 ± 0.02	172.361 ± 0.026	-0.13 ± 0.03
1.33 ± 0.13	301.809 ± 0.166	-0.74 ± 0.08	0.91 ± 0.02	173.475 ± 0.039	-0.1 ± 0.03
1.09 ± 0.11	302.255 ± 0.146	-0.76 ± 0.07	0.66 ± 0.01	174.932 ± 0.043	-0.12 ± 0.02
0.89 ± 0.11	302.632 ± 0.182	-0.7 ± 0.07	0.5 ± 0.01	176.003 ± 0.036	-0.1 ± 0.02
0 ± 0.06	304.126 ± 0.065	0 ± 0.04	0 ± 0.01	179.426 ± 0.008	0 ± 0.01

Table S5: P, V and t data for Fa100 and NaCl. d spacings are listed in file `fa100.csv`.

P (GPa)	V (Å^3)	t_{Fa100} (GPa)	P_{NaCl} (GPa)	V_{NaCl} (Å^3)	t_{NaCl} (GPa)
0.01 ± 0.06	307.763 ± 0.119	0.01 ± 0.02	0.018 ± 0.034	179.49 ± 0.019	0 ± 0.01
0.47 ± 0.08	306.67 ± 0.078	0 ± 0.03	0.4 ± 0.04	176.847 ± 0.031	0.1 ± 0.01
1.2 ± 0.12	305.431 ± 0.068	0.26 ± 0.04	1.25 ± 0.05	171.634 ± 0.024	0.18 ± 0.03
1.93 ± 0.13	303.896 ± 0.081	0.48 ± 0.06	2.12 ± 0.05	167.111 ± 0.022	0.2 ± 0.02
2.65 ± 0.14	302.29 ± 0.182	0.65 ± 0.06	2.93 ± 0.06	163.385 ± 0.022	0.23 ± 0.03
3.4 ± 0.16	300.986 ± 0.11	0.81 ± 0.07	3.79 ± 0.07	159.904 ± 0.024	0.22 ± 0.02
3.97 ± 0.18	299.787 ± 0.136	0.96 ± 0.09	4.44 ± 0.07	157.518 ± 0.021	0.25 ± 0.02
4.52 ± 0.19	298.608 ± 0.164	1.1 ± 0.09	5.09 ± 0.08	155.309 ± 0.023	0.24 ± 0.02
3.23 ± 0.14	300.743 ± 0.118	-0.69 ± 0.06	2.86 ± 0.06	163.713 ± 0.022	-0.13 ± 0.03
3.32 ± 0.18	300.966 ± 0.115	-0.71 ± 0.07	2.94 ± 0.07	163.346 ± 0.035	-0.13 ± 0.03
4.73 ± 0.16	297.96 ± 0.086	-0.2 ± 0.06	4.5 ± 0.07	157.301 ± 0.022	0.15 ± 0.03
4.97 ± 0.17	297.358 ± 0.116	-0.26 ± 0.06	4.86 ± 0.08	156.057 ± 0.02	-0.1 ± 0.03
4.76 ± 0.16	297.817 ± 0.106	-0.3 ± 0.06	4.64 ± 0.07	156.815 ± 0.019	-0.12 ± 0.03
4.64 ± 0.16	297.86 ± 0.12	-0.31 ± 0.06	4.51 ± 0.07	157.28 ± 0.015	-0.11 ± 0.03
4.23 ± 0.17	298.641 ± 0.101	-0.4 ± 0.07	4.06 ± 0.06	158.897 ± 0.013	-0.14 ± 0.04
4.02 ± 0.15	299.322 ± 0.116	-0.41 ± 0.06	3.83 ± 0.07	159.771 ± 0.026	-0.13 ± 0.03
3.66 ± 0.15	300.094 ± 0.123	-0.52 ± 0.04	3.41 ± 0.07	161.413 ± 0.035	-0.15 ± 0.04
3.39 ± 0.15	300.543 ± 0.11	-0.46 ± 0.06	3.16 ± 0.07	162.422 ± 0.031	-0.12 ± 0.03
2.99 ± 0.15	301.406 ± 0.114	-0.57 ± 0.05	2.71 ± 0.06	164.385 ± 0.027	-0.15 ± 0.03
2.75 ± 0.14	301.89 ± 0.101	-0.53 ± 0.05	2.45 ± 0.06	165.528 ± 0.029	-0.08 ± 0.03
2.15 ± 0.13	303.154 ± 0.109	-0.63 ± 0.06	1.82 ± 0.05	168.593 ± 0.026	-0.14 ± 0.02
1.86 ± 0.11	303.71 ± 0.094	-0.59 ± 0.04	1.53 ± 0.05	170.115 ± 0.025	-0.09 ± 0.03
1.59 ± 0.15	304.296 ± 0.107	-0.64 ± 0.07	1.24 ± 0.05	171.7 ± 0.026	-0.11 ± 0.03
1.41 ± 0.13	304.715 ± 0.101	-0.61 ± 0.06	1.06 ± 0.04	172.735 ± 0.024	-0.09 ± 0.02
1.1 ± 0.12	305.672 ± 0.169	-0.62 ± 0.06	0.76 ± 0.04	174.537 ± 0.026	-0.11 ± 0.02
0.94 ± 0.13	305.972 ± 0.147	-0.58 ± 0.06	0.62 ± 0.04	175.381 ± 0.025	-0.11 ± 0.02
-0.02 ± 0.08	307.981 ± 0.233	0.05 ± 0.06	$(1 \pm 0.1)10^{-4}$	179.62 ± 0.035	0.02 ± 0.01

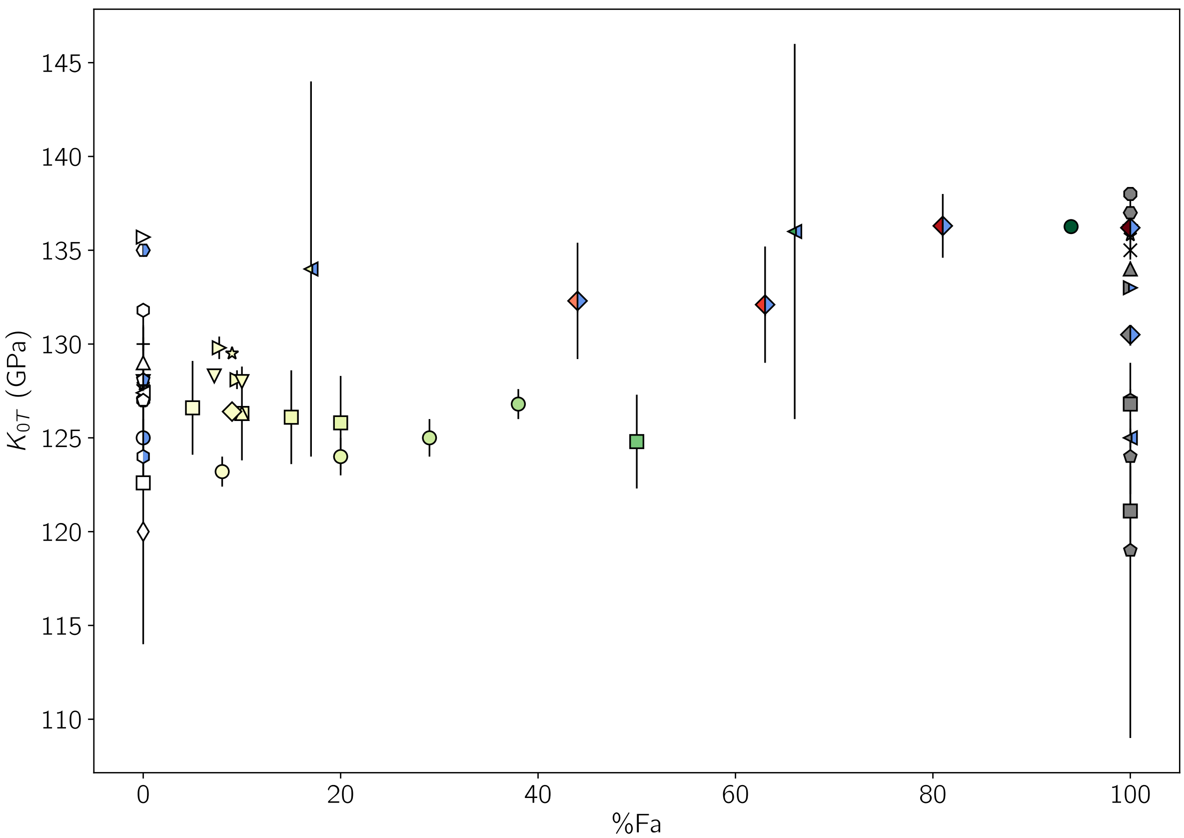

Figure S4: Bulk moduli of olivines as a function of their Fa content. Note that these K values are reported as published, *i.e.* obtained with values of dK/dP that may differ. Therefore care should taken when doing a comparison. All data on this figure are listed in Table S6.

Table S6: K and dK/dP from previous works. Data is presented as published, for example, in the case of Nestola et al. (2011) data have not been recalculated with the new Quartz pressure scale (Scheidl et al., 2016).

X_{Fe} (%)	K_T (GPa)	dK/dP	Ref.
			Experimental data
0	127.5	5.39	Kumazawa and Anderson (1969)
0	127 ± 0.25	5.07 ± 0.27	Chung (1971)
0	135	4	Hazen (1976)
0	120 ± 6	5.6 ± 0.7	Olinger (1977)
0	131.8	3.4	Syono et al. (1981)
0	124	4	Syono et al. (1981)
0	113	5	Syono et al. (1981)
0	127.84		Suzuki et al. (1983)
0	122.6	4.3	Kudoh and Takéuchi (1985)
0	135.7 ± 1.0	$3.98 \pm .0.1$	Will et al. (1986)
0	127.4	4.8	Isaak et al. (1989)
0	128 ± 0.8	4	Andrault et al. (1995)
0	129 ± 1	4.2 ± 0.2	Duffy et al. (1995)
0	125 ± 2	4.0 ± 0.4	Downs et al. (1996)
0	127 ± 4	4.2 ± 0.8	Zhang (1998)
0	128.1 ± 4	4	Zhang (1998)
0	130 ± 0.9	4.12 ± 0.7	Finkelstein et al. (2014)
5	126.6 ± 2.5	5.11 ± 0.27	Chung (1971)
7.2	128.3	5.16	Kumazawa and Anderson (1969)
7.7	129.8 ± 0.6		Isaak (1992)
8	123.2 ± 0.8	5.6 ± 0.2	Nestola et al. (2011)
9	129.5	4.5	Webb (1989)
9.5	128.1 ± 0.5		Isaak (1992)
10	126.3 ± 2.5	5.16 ± 0.27	Chung (1971)
10	128 ± 0.2	3.8 ± 0.2	Zha et al. (1996)
10	126.3	4.28	Abramson et al. (1997)

Continues on next page

Table S6 – *Continued from previous page*

X_{Fe} (%)	K_T (GPa)	dK/dP	Ref.	Comments
8–10	126.4 ± 0.2	4.51 ± 0.05	Angel et al. (2017)	BM3-isothermal
15	126.1 ± 2.5	5.16 ± 0.27	Chung (1971)	
17	134 ± 10	4	Andrault et al. (1995)	
20	125.8 ± 2.5	5.27 ± 0.28	Chung (1971)	
20	124 ± 1	5.4 ± 0.3	Nestola et al. (2011)	
29	125 ± 1	5.1 ± 0.3	Nestola et al. (2011)	
38	126.8 ± 0.8	5.2 ± 0.2	Nestola et al. (2011)	
50	124.8 ± 2.5	5.48 ± 0.29	Chung (1971)	
66	136 ± 10	4	Andrault et al. (1995)	
92	130.5	4	Kudoh and Takeda (1986)	Mn
100	124 ± 2	4	Mao et al. (1969)	
100	121.1 ± 2.4	5.97 ± 0.32	Chung (1971)	
100	119 ± 10	7 ± 4	Yagi et al. (1975)	
100	124 ± 2	5	Yagi et al. (1975)	
100	138	5	Smyth (1975)	
100	137		Sumino (1979)	
100	127 ± 0.6	5.2 ± 0.4	Graham et al. (1988)	
100	135.8 ± 1.3		Wang et al. (1989)	
100	126.8	5	Hofmeister et al. (1989)	
100	123.9 ± 4.6	5.0 ± 0.8	Williams et al. (1990)	
100	103.8	7.1	Plymate and Stout (1990)	400°C
100	134 ± 0.4		Isaak et al. (1993)	
100	125 ± 0.5	4	Andrault et al. (1995)	
100	136 ± 3	4.1 ± 0.7	Zhang (1998)	
100	136.26 ± 0.21	4.88 ± 0.05	Speziale et al. (2004)	
100	135 fixed	4.0 ± 0.2	Zhang et al. (2017)	

X_{Fe} (%)	K_T (GPa)	dK/dP	Ref.	
		Theoretical calculations		
0	134.4 ± 0.7	3.88 ± 0.88	Brodholt et al. (1996)	
0	136.8		Núñez-Valdez et al. (2010)	
0	126.54	4.3	Núñez-Valdez et al. (2013)	
12.5	139–140.6		Núñez-Valdez et al. (2010)	Fe in M(1) or M(2) site
12.5	129.54	4.7	Núñez-Valdez et al. (2013)	
100	139		Stackhouse et al. (2010)	
	147			
	151			

References

Abramson, E. H., Brown, J. M., Slutsky, L. J., Zaug, J., 1997. The elastic constants of San Carlos olivine to 17 GPa. J. Geophys. Res. 102 (B6), 12,253–12,263.

Andrault, D., Bouhifd, M., Itié, J., Richet, P., 1995. Compression and amorphization of $(Mg,Fe)_2SiO_4$ olivines: An X-ray diffraction study up to 70 GPa. Phys Chem Minerals 22 (2), 99–107.

Angel, R. J., Alvaro, M., Nestola, F., 2017. 40 years of mineral elasticity: a critical review and a new parameterisation of equations of state for mantle olivines and diamond inclusions. Phys Chem Minerals 102, 1–19.

Brodholt, J., Patel, A., Refson, K., 1996. An ab initio study of the compressional behavior of forsterite. Am. Mineral. 81, 257–260.

Chung, D. H., 1971. Elasticity and equations of state of olivines in the Mg_2SiO_4-Fe_2SiO_4 system. Geophys. J. Int. 25 (5), 511–538.

Downs, R., Zha, C., Duffy, T., Finger, L., 1996. The equation of state of forsterite to 17.2 GPa and effects of pressure media. Am. Mineral. 81 (1-2), 51–55.

Duffy, T. S., Zha, C.-S., Downs, R. T., Mao, H.-k., Hemley, R. J., 1995. Elasticity of forsterite to 16 GPa and the composition of the upper mantle. Nature 378 (6553), 170–173.

Finkelstein, G. J., Dera, P. K., Jahn, S., Oganov, A. R., Holl, C. M., Meng, Y., Duffy, T. S., 2014. Phase transitions and equation of state of forsterite to 90 GPa from single-crystal X-ray diffraction and molecular modeling. Am. Mineral. 99 (1), 35–43.

Graham, E. K., Schwab, J. A., Sopkin, S. M., Takei, H., 1988. The pressure and temperature dependence of the elastic properties of single-crystal Fayalite Fe_2SiO_4. Phys Chem Minerals 16 (2), 186–198.

Hazen, R. M., 1976. Effects of temperature and pressure on the crystal structure of Forsterite. Am. Mineral. 61, 1280–1293.

Hofmeister, A. M., Xu, J., Mao, H.-k., Bell, P. M., Hoering, T. C., 1989. Thermodynamics of Fe-Mg olivines at mantle pressures; mid- and far-infrared spectroscopy at high pressure. Am. Mineral. 74 (3-4), 281–306.

Isaak, D. G., 1992. High-temperature elasticity of iron-bearing olivines. J. Geophys. Res. 97 (B2), 1871–1885.

Isaak, D. G., Anderson, O. L., Goto, T., Suzuki, I., 1989. Elasticity of single-crystal forsterite measured to 1700 K. J. Geophys. Res. 94 (B5), 5895–5906.

Isaak, D. G., Graham, E. K., Bass, J. D., Wang, H., 1993. The elastic properties of single-crystal fayalite as determined by dynamical measurement techniques. Pure appl. geophys. 141 (2-4), 393–414.

Kudoh, Y., Takeda, H., 1986. Single crystal X-ray diffraction study on the bond compressibility of fayalite, Fe_2SiO_4 and rutile, TiO_2 under high pressure. Physica B+C 139–140, 333–336.

Kudoh, Y., Takéuchi, Y., 1985. The crystal structure of forsterite Mg_2SiO_4 under high pressure up to 149 kb. Zeitschrift für Kristallographie - Crystalline Materials 171 (1-4), 291–302.

Kumazawa, M., Anderson, O. L., 1969. Elastic Moduli, Pressure Derivatives, and Temperature Derivatives of Single-Crystal Olivine and Single-Crystal Forsterite. J. Geophys. Res. 74 (25), 5961–5972.

Mao, H.-k., Takahashi, T., Bassett, W. A., Weaver, J. S., Akimoto, S.-i., 1969. Effect of pressure and temperature on the molar volumes of Wüstite and of three $(Fe, Mg)_2SiO_4$ spinel solid solutions. J. Geophys. Res. 74 (4), 1061–1069.

Nestola, F., Pasqual, D., Smyth, J. R., Novella, D., Secco, L., Manghnani, M. H., Dal Negro, A., 2011. New accurate elastic parameters for the forsterite-fayalite solid solution. Am. Mineral. 96 (11-12), 1742–1747.

Núñez-Valdez, M., Umemoto, K., Wentzcovitch, R. M., 2010. Fundamentals of elasticity of $(Mg_{1=x}, Fe_x)_2SiO_4$ olivine. Geophys. Res. Lett. 37 (14), n/a–n/a.

Núñez-Valdez, M., Wu, Z., Yu, Y. G., Wentzcovitch, R. M., 2013. Thermal elasticity of $(Fe_x,Mg_{1=x})_2SiO_4$ olivine and wadsleyite. Geophys. Res. Lett. 40 (2), 290–294.

Olinger, B., 1977. Compression studies of forsterite (Mg_2SiO_4) and enstatite ($MgSiO_3$). In: Manghnani, M. H., Akimoto, S.-i. (Eds.), High-Pressure Research. Academic Press, pp. 325–334.

Plymate, T., Stout, J., 1990. Pressure-volume-temperature behavior of fayalite based on static compression measurements at 400°C. Phys Chem Minerals 17 (3).

Scheidl, K. S., Kurnosov, A., Trots, D. M., Boffa Ballaran, T., Angel, R. J., Miletich, R., 2016. Extending the single-crystal quartz pressure gauge up to hydrostatic pressure of 19 GPa. Journal of Applied Crystallography 49 (6), 2129–2137.

Smyth, J. R., 1975. High temperature crystal chemistry of Fayalite. Amer. Mineral. 60, 1092–1097.

Speziale, S., Duffy, T. S., Angel, R. J., 2004. Single-crystal elasticity of fayalite to 12 GPa. J. Geophys. Res. 109 (B12), 15.

Stackhouse, S., Stixrude, L., Karki, B., 2010. Determination of the high-pressure properties of fayalite from first-principles calculations. Earth Planet Sc Lett 289 (3-4), 449–456.

Sumino, Y., 1979. The elastic constants of Mn_2SiO_4, Fe_2SiO_4 and Co_2SiO_4, and the elastic properties of olivine group minerals at high temperature. J. Phys. Earth 27 (3), 209–238.

Suzuki, I., Anderson, O. L., Sumino, Y., 1983. Elastic properties of a single-crystal forsterite Mg_2SiO_4, up to 1,200 K. Phys Chem Minerals 10 (1), 38–46.

Syono, Y., Goto, T., Sato, J. i., Takei, H., 1981. Shock compression measurements of single-crystal forsterite in the pressure range 15–93 GPa. J. Geophys. Res. 86 (B7), 6181–6186.

Wang, H., Bass, J. D., Rossman, G. R., 1989. Elastic properties of Fe-bearing pyroxenes and olivines. Eos Trans. AGU 70, 474.

Webb, S., 1989. The elasticity of the upper mantle orthosilicates olivine and garnet to 3 GPa. Phys Chem Minerals 16 (7), 684–692.

Weidner, D. J., Vaughan, M. T., Wang, L., Long, H., Li, L., Dixon, N. A., Durham, W. B., 2010. Precise stress measurements with white synchrotron x rays. Rev. Sci. Instrum. 81 (1), 013903.

Will, G., Hoffbauer, W., Hinze, E., Lauterjung, J., 1986. The compressibility of forsterite up to 300 kbar measured with synchrotron radiation. Physica B+C 139-140, 193–197.

Williams, Q., Knittle, E., Reichlin, R., Martin, S., Jeanloz, R., 1990. Structural and electronic properties of Fe_2SiO_4-fayalite at ultrahigh pressures: Amorphization and gap closure. J. Geophys. Res. 95 (B13), 21,549–21,563.

Yagi, T., Ida, Y., Sato, Y., Akimoto, S.-i., 1975. Effect of hydrostatic pressure on the lattice parameters of Fe_2SiO_4 olivine up to 70 kbar. Phys. Earth Planet. Int. 10 (4), 348–354.

Zha, C.-S., Duffy, T. S., Downs, R. T., Mao, H.-k., Hemley, R. J., 1996. Sound velocity and elasticity of single-crystal forsterite to 16 GPa. J. Geophys. Res. 101 (B8), 17535–17545.

Zhang, J. S., Hu, Y., Shelton, H., Kung, J., Dera, P., 2017. Single-crystal X-ray diffraction study of Fe_2SiO_4 fayalite up to 31 GPa. Phys Chem Minerals 44 (3), 171–179.

Zhang, L., 1998. Single crystal hydrostatic compression of (Mg, Mn, Fe, Co)$_2$SiO$_4$ olivines. Phys Chem Minerals 25 (4), 308–312.